JOURNAL OF MATERIALS SCIENCE 28 (1993) 2089–2096

Effects of heat treatments on the microstructure of a yttria/alumina-doped hot-pressed Si_3N_4 ceramic

C. T. BODUR
Department of Materials Science, University of Technology, 15-73 Broadway, Sydney, Australia

D. V. SZABÓ
Max-Planck-Institut für Metallforschung, Institut für Werkstoffwissenschaft, Seestrasse 92, D-7000 Stuttgart 1, Germany

K. KROMP
Institut für Festkörperphysik der Universität Wien, Strudlhofgasse 4, A-1090 Wien, Austria

The effects of post-sintering heat treatments on the microstructure in an Y_2O_3–Al_2O_3-doped hot-pressed silicon nitride ceramic in an argon atmosphere were studied. The degree of crystallization of the secondary crystalline phase depended more on the time than the temperature of the heat treatments. Analytical transmission electron microscopy studies revealed a spencite-(Y, N)-apatite solid solution as the secondary crystalline phase, while the aluminium content in the residual glass was high.

1. Introduction

Silicon nitride is among the most promising structural ceramic materials for high-temperature application. The microstructure of hot-pressed silicon nitride ceramics usually consists of β-Si_3N_4 as the major crystalline phase, secondary crystalline phase(s) and an amorphous grain-boundary phase resulting from the liquid-phase sintering process [1–3]. The intergranular amorphous phase includes sintering additives such as MgO, Al_2O_3 or Y_2O_3 as well as impurity elements such as calcium, sodium, potassium and iron [2, 4]. Relatively high amounts of impurities can have profound effects on the high-temperature properties of this material by decreasing the viscosity of the amorphous phase [5, 6]. At high temperatures ($\geq$ 1000 °C) this amorphous phase behaves viscoelastically [7] and controls various properties such as creep, subcritical crack growth or oxidation behaviour. In order to avoid amorphous-phase-induced high-temperature property degradation of this material, the amorphous grain-boundary phase can be crystallized by a post-fabrication heat treatment at high temperatures [8–11]. Different crystalline phases such as (Y, N)-apatite [9], Y-Al-garnet (YAG) [11] or cordierite [11] can be produced, depending on the chemical composition of the original amorphous grain-boundary phase.

This study was performed to investigate various states of crystallization of the amorphous grain-boundary phase in an Y_2O_3–Al_2O_3-doped hot-pressed silicon nitride and the dependence on different heat treatments in an argon atmosphere. The phases were identified by X-ray diffraction, whereas the microstructural and microanalytical characterization were performed by scanning electron and analytical transmission electron microscopy.

2. Experimental procedure

2.1. Material and heat treatments

The material for this investigation was an 8 wt% Y_2O_3–2 wt% Al_2O_3-doped hot-pressed silicon nitride which was supplied (ESK Kempten, Germany) in rectangular bars of $3.5 \times 7 \times 32$ mm^3. As can be seen in Table I, a relatively high calcium concentration in the starting Si_3N_4 powder has to be considered in this study.

The heat treatments were performed in a high-vacuum chamber which was first evacuated to about 5×10^{-6} mbar and then floated with argon gas (purity 99.999%) to a pressure of 1200 mbar. The specimens were heated indirectly to the desired temperature by a graphite susceptor in a water-cooled copper induction coil [12]. Table II summarizes the different heat treatments of the material studied in this paper.

2.2. X-ray diffraction (XRD) analysis

The material was investigated by an X-ray diffraction method (Guinier diffractometry with Cu$K_{\alpha 1}$ radiation) in powdered form to analyse the amount and the variety of the crystalline phases. The phases were identified by comparing the obtained diffractograms with available ASTM standards.

0022–2461

TABLE I Manufacturer's data of the starting powder

	Element							
	N_2	O_2	C	Ca	Al	Fe	Mg	Si
wt %	37.9	1.9	0.3	0.25	0.22	0.2	0.08	bal.

Grain size: 97% < 10.6 μm; 50% < 1.6 μm; 6% < 0.6 μm.
Specific surface area: 6.1 m^2g^{-1}.
Modification: 96% α-Si_3N_4, 4% β-Si_3N_4.
Additives: 8 wt % Y_2O_3, 2 wt % Al_2O_3.

TABLE II Features of the investigated material

Material state	Heat treatment	Controlled crack-growth experiments
1	As-received	20 °C, 1 h, air
2	As-received	1200 °C, 5 h, argon
3	1400 °C, 10 h, + 1300 °C, 10 h,	1200 °C, 4 h, argon
4	1360 °C, 30 h	1200 °C, 4 h, argon
5	1300 °C, 40 h	1200 °C, 4 h, argon

2.3. Scanning electron microscopy

Scanning electron microscopy (JSM 35, Jeol, Tokyo, Japan) was used to analyse the morphology of the phases. The volume percentage of the amorphous grain-boundary phase was determined with a point-counting method [13] to quantify the degree of crystallization as a function of the heat treatments.

The specimens were first polished to a 6 μm finish and then etched in a 50 wt % NaOH + 50 wt % KOH solution at 360 °C for 1 min to distinguish the amorphous phase from the β-Si_3N_4 grains in the scanning electron micrographs.

2.4. Transmission electron microscopy

The microstructural and microanalytical investigations were performed with a transmission electron microscope (JEM 2000 FX, Jeol, Tokyo, Japan), operating at 200 kV and equipped with an X-ray energy dispersive (Si-Li) spectrometer (EDS) with beryllium-window (Tracor TN 2000, Tracor Northern, Middletown, WI) and an electron energy loss spectrometer (EELS) (Gatan 607, Gatan Inc. Warrendale, PA). The conventional imaging and selected-area diffraction modes were used to characterize the microstructure and to determine the phases. The cation composition of the different phases was analysed by EDS, while the anions (N, O) in the secondary crystalline phase were determined qualitatively by EELS.

For the TEM investigations a standard specimen preparation technique for ceramic materials was used. Cylinders of 3 mm diameter were cut with an ultrasonic drill from the bulk material. These cylinders were cut to discs, ground to a thickness of 100 μm and dimpled. Then the specimens were thinned by ion-milling at an incidence angle of 12° at 6 kV. Finally the specimens were coated with a thin carbon layer to avoid surface charging by the electron beam.

3. Results and discussion

3.1. Fracture surface investigations

After the heat treatments the surface of the specimens became porous and easily abraded, especially for the material heat treated at temperatures higher than 1360 °C. In a previous paper the surface morphology was described in detail [12].

The internal morphology of the specimens had also changed. Fig. 1a and b show the fracture surfaces from the controlled slow crack growth region [14] of the material in States 2 (as-received) and 5 (1300 °C, 40 h), respectively. The morphology of the as-received specimens fracture surface (Fig. 1a) appears more regular than that of the heat-treated specimen (Fig. 1b). In Fig. 1a, single large β-Si_3N_4 grains up to a length of 10 μm are visible. In Fig. 1b the grains are homogeneous in size, and clusters of small equiaxed Si_3N_4 grains can be seen.

3.2. X-ray diffraction analysis

The X-ray diffractrometry identified the same crystalline phases in all of the heat-treated and also in the as-received material. Hexagonal β-Si_3N_4 with the lattice parameters $a = 0.7608$ nm and $c = 0.291\ 09$ nm was observed as the main crystalline phase (90–95 vol % of the total amount). The secondary crystalline phase was identified as one of the Y–Si–O–N phases listed below.

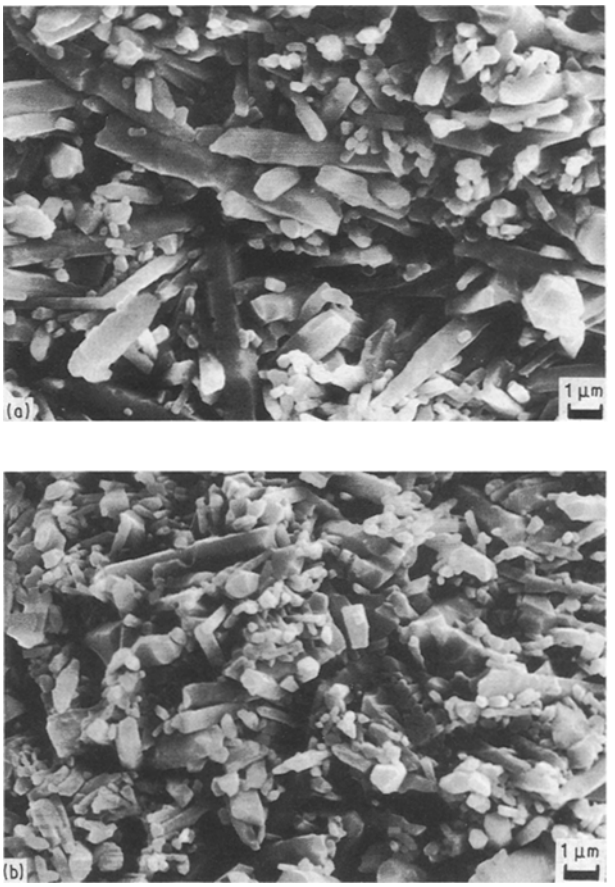

Figure 1 Scanning electron micrographs of the fracture surface after the controlled crack-growth experiments ($\dot{\delta} = 5$ μm min^{-1}). (a) As-received, State 2; (b) 1300 °C, 40 h, State 5.

(i) $Y_5N\ (SiO_4)_3$: yttrium nitride silicate ((Y, N)-apatite) hexagonal with $a = 0.941$ nm, $c = 0.676$ nm (ASTM 33-1459).

(ii) $Si_3N_4 \cdot 10\ Y_2O_3 \cdot 9\ SiO_2$: yttrium silicon oxide nitride, hexagonal with $a = 0.940$ nm, $c = 0.680$ nm (ASTM 30-1462).

(iii) $Y_{4.67}\ (SiO_4)_3\ O$: yttrium oxide silicate, hexagonal with $a = 0.9347$ nm, $c = 0.6727$ nm (ASTM 30-1457) which is an oxidation product of yttrium nitride silicate [15].

3.3. Scanning electron microscopy

The result of the quantitative phase analysis of the amorphous phase is demonstrated by Fig. 2. As was expected, longer heating times and higher temperatures during the heat treatments resulted in a decrease of the amorphous phase content. In addition, the controlled crack-growth experiments in argon at 1200 °C for ~4–5 h can be considered as a heat treatment (see Table II), decreasing the amorphous phase content in the as-received material by about 60 vol %. In comparison, a heat treatment at 1360 °C for 30 h increases the secondary crystalline phase content up to 75 vol % (relative to the amorphous phase content). Representative scanning electron micrographs are shown in Fig. 3a and b.

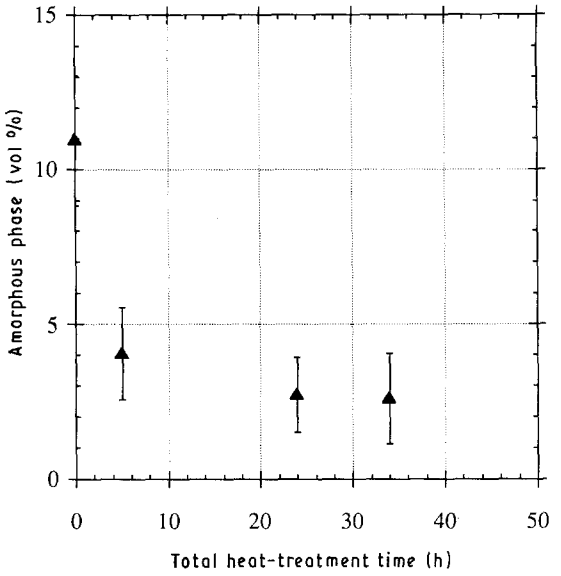

Figure 2 The volume fraction of the amorphous grain-boundary phase after different heat treatments.

3.4. Transmission electron microscopy

The as-received material (State 1) consisted of small and large hexagonal β-Si_3N_4 grains with diameters of 0.2–1 μm, embedded in a highly electron-absorbing amorphous phase shown in Fig. 4. The dark-field micrograph reveals the amorphous grain-boundary phase between Si_3N_4 grains and at triple points (bright regions in Fig. 4). After the controlled crack-growth experiment in argon at 1200 °C for 5 h, a partial crystallization of the secondary phase was found in the as-received material. Fig. 5 shows a planar growth front of this crystalline secondary phase with the corresponding electron diffraction pattern inserted. The growth direction is parallel to $\langle 10\bar{1}0 \rangle$, the growing planes are parallel to $\{10\bar{1}0\}$-planes. The growth of this secondary crystalline phase is strongly anisotropic.

After a heat treatment of 20 h, large regions of residual amorphous phase in triple points and between the crystalline phases were present (Fig. 6). Bending contours, resulting from inner stresses in the material are visible in β-Si_3N_4 grains. After a heat treatment of 30 h, crystalline pockets could be found, nearly fully crystallized (Fig. 7). The dislocation network (arrowed) at the Si_3N_4–Si_3N_4 grain boundary and the dislocations in the Si_3N_4 grains are probably due to the crystallization of the amorphous grain-boundary phase [16], but could also have their origin in the controlled crack growth experiments.

The transmission electron micrographs (Figs 5–7) indicate that, in most of the cases, crystalline pockets contain only one single-crystalline grain. The grain size of the secondary phase is as large as or larger than the silicon nitride grains, but a large-grained interconnected structure, as seen in garnet [11], was not found in this system.

By EDS measurements it could be shown that the average composition of Si_3N_4 does not change during

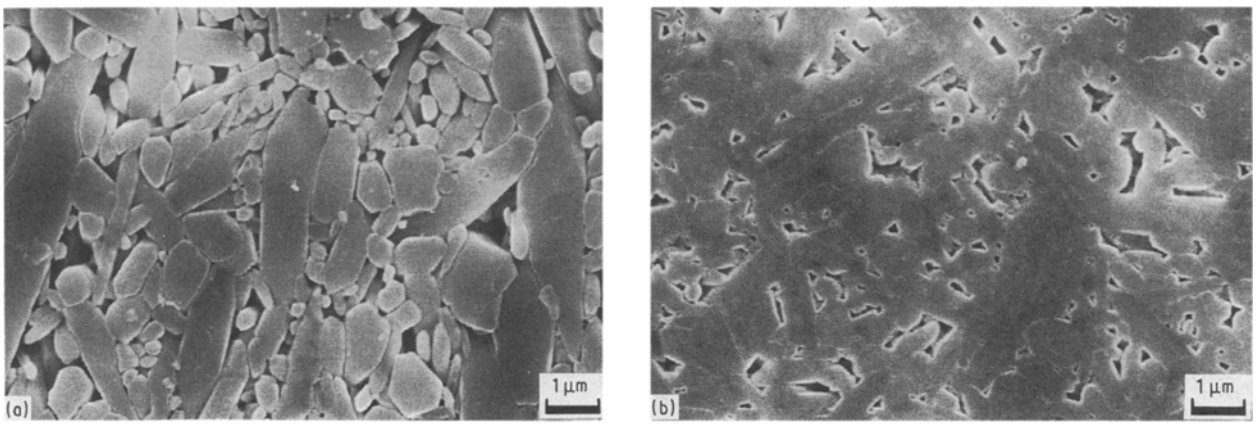

Figure 3 Scanning electron micrographs of the polished and etched surfaces, showing the phases (amorphous or crystalline) for the quantitative phase analysis. (a) As-received, State 1; (b) 1400 °C, 10 h + 1300 °C, 10 h, State 3.

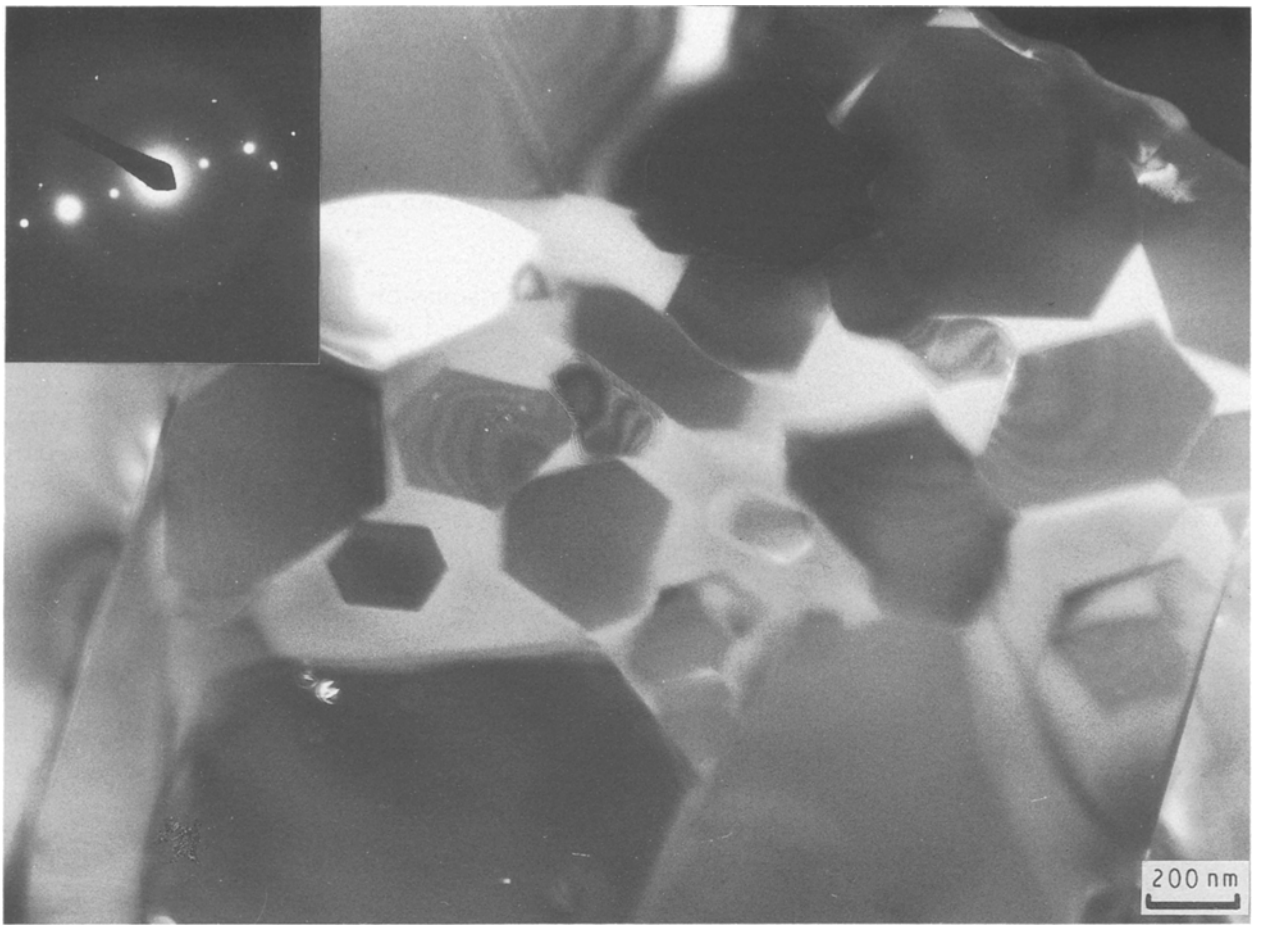

Figure 4 TEM diffuse dark-field micrograph of the general microstructure of the as-received material.

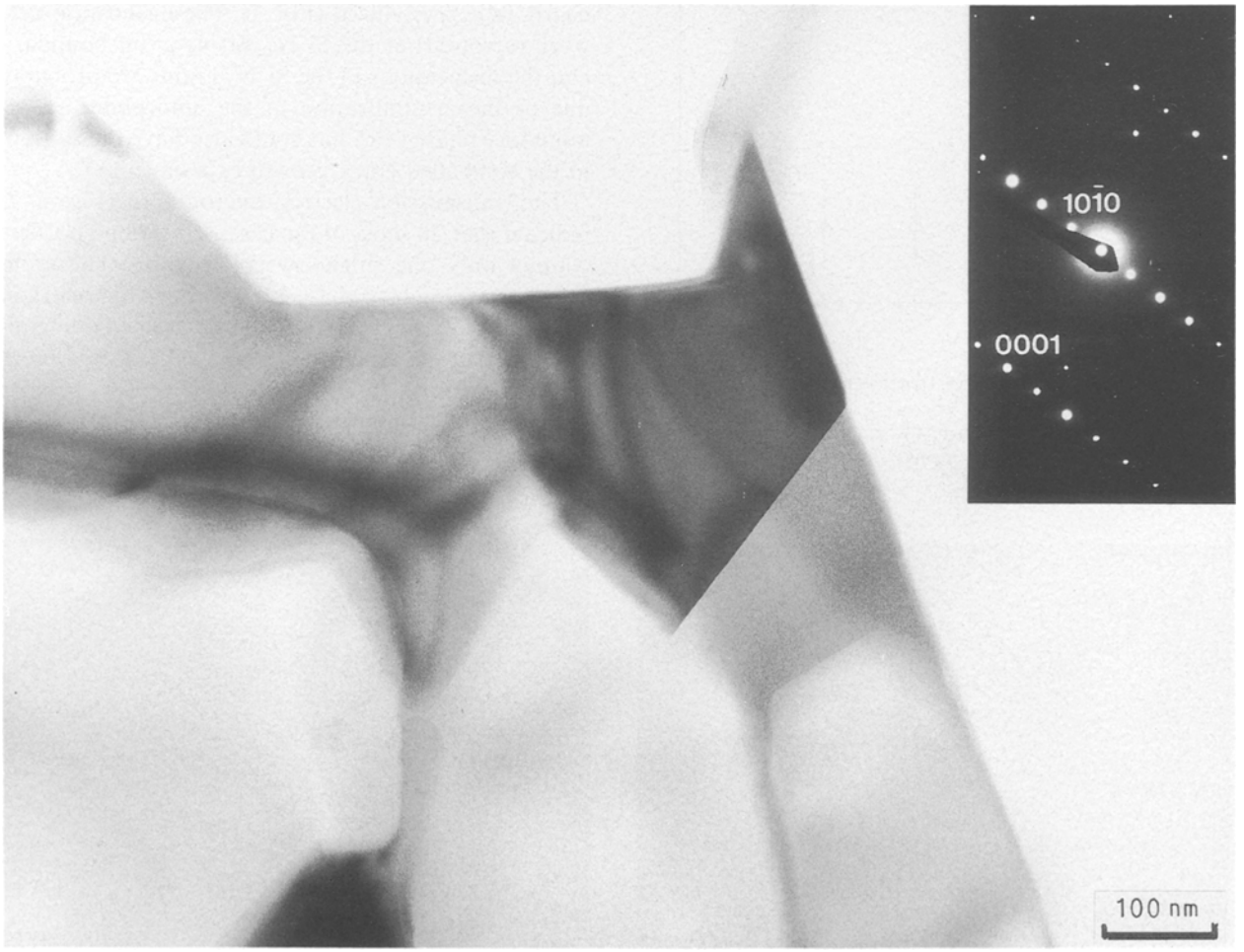

Figure 5 TEM bright-field micrograph of a planar growth front of the secondary crystalline phase, as-received material after controlled crack- growth experiments, 1200 °C, 5 h; State 2.

Figure 6 The microstructure of the silicon nitride ceramic after a heat treatment of 20 h consists of residual amorphous grain-boundary phase (arrows), silicon nitride grains and secondary crystalline phase (Y).

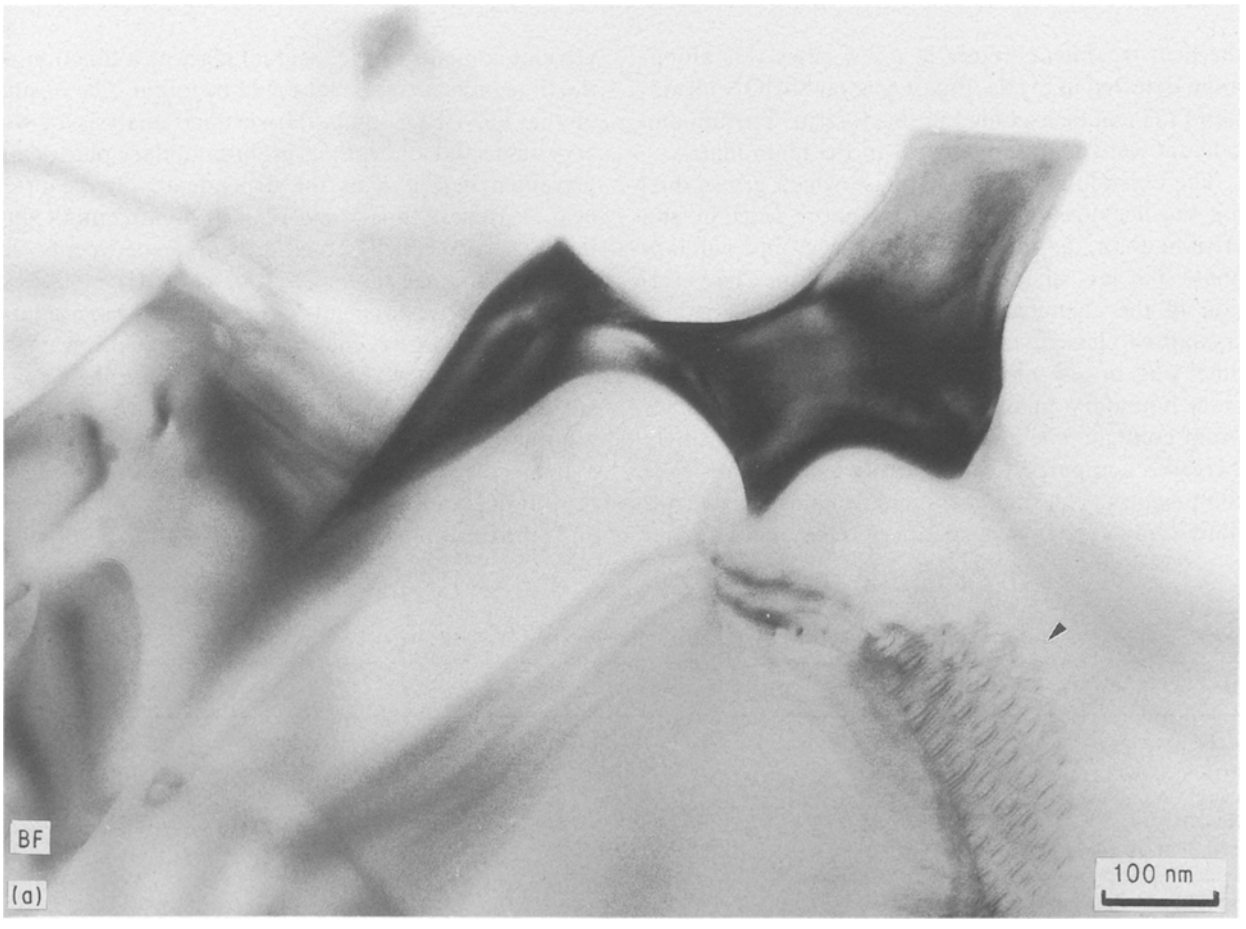

Figure 7 TEM (a) bright-field and (b) dark-field micrographs of a single crystalline pocket, 1360 °C, 30 h, State 4.

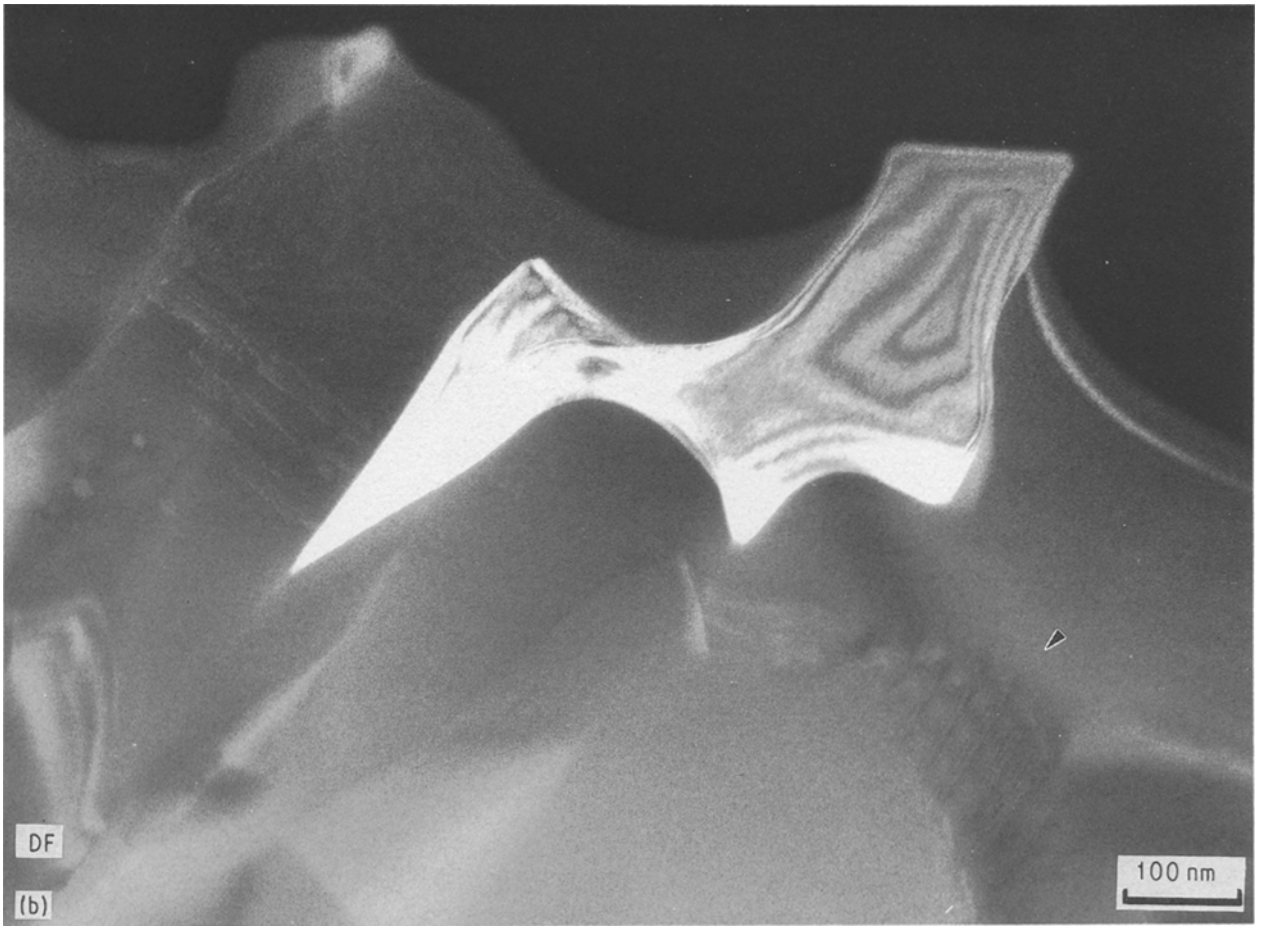

Figure 7 Continued

the heat treatments. Only in a few cases was aluminium detected in Si_3N_4, thus a general SiAlON formation [17] can be excluded in this system. Yttrium and calcium were also not detected in the main matrix.

The crystalline secondary phase which grows during the heat treatments contains more calcium and yttrium than the initial amorphous grain-boundary phase, but less silicon and no aluminium. The variation of the chemical composition of the secondary crystalline phase as a function of the heat-treatment time was not significant. The residual amorphous grain-boundary phase has a lower calcium and yttrium content. The amount of aluminium is strongly increased compared to the starting amorphous phase composition. The silicon content remains nearly constant. Only a weak dependence of the aluminium and yttrium contents in the residual glass as a function of the time of heat treatment could be found. The results of the TEM/EDS quantitative microanalysis of the crystalline and amorphous grain-boundary phases are presented in Fig. 8 as the dependence on the total heat-treatment time (time of heat treatment(s) plus time of controlled crack-growth experiments at 1200 °C), and are summarized in Table III.

By EELS measurements of the crystalline secondary phase O*K* and Ca*L* lines could be detected but no N was found (Fig. 9). A minor YM_1 edge lies at an energy loss of 394 eV, which overlaps with the background of the N*K* edge at 401 eV.

From the literature [17] it is known that spencite ($Y_4Ca(SiO_4)_3O$) shows similar diffraction patterns and unit-cell dimensions to the (Y, N)-apatite. It is also

TABLE III Average composition of the cations (at %) of the different grain-boundary phases

Phase	Si	Al	Y	Ca
Initial amorphous grain-boundary phase	44.44 ± 1.86	9.12 ± 1.76	43.51 ± 1.46	2.93 ± 0.45
Secondary crystalline phase	37.07 ± 1.22	none	58.31 ± 1.22	4.62 ± 0.19
Residual amorphous grain-boundary phase	43.37 ± 1.12	22.40 ± 1.41	32.16 ± 1.55	1.33 ± 0.26

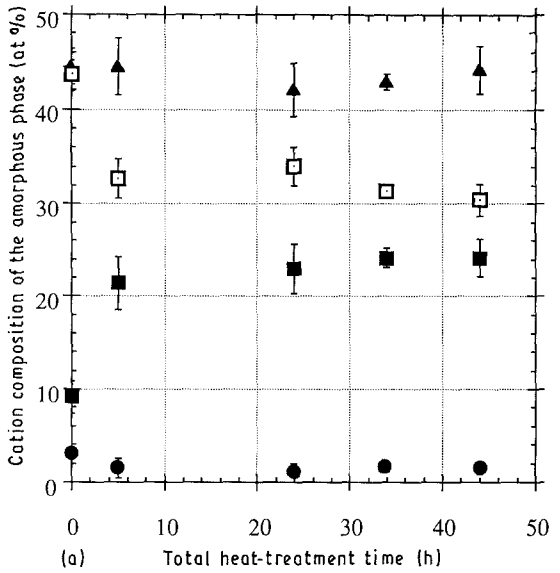

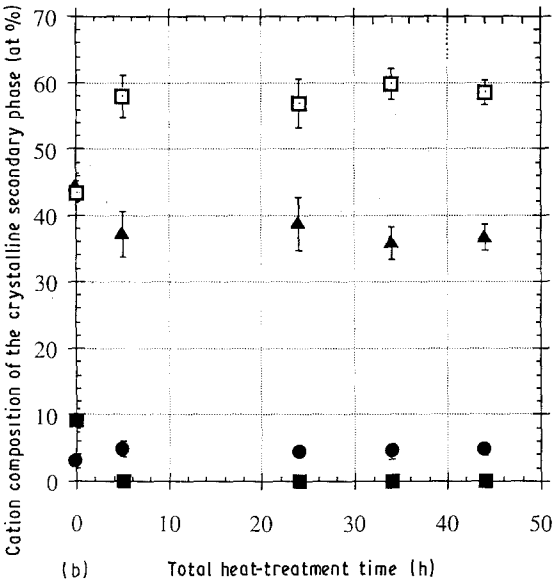

Figure 8 Cation composition (at %) of the grain-boundary phase after different heat treatments: (a) amorphous grain-boundary phase; (b) secondary crystalline phase. As a reference point the composition of the initial grain-boundary phase (time = 0 h, material State 1) is shown in both cases. (▲) Si, (■) Al, (⊡) Y, (●) Ca.

well known [18] that (Y, N)-apatite is isostructural with an alumino-silicate and therefore is able to dissolve impurities like calcium. Comparing the measured average atomic ratios (Y + Ca) /Si in the secondary crystalline phase of 1.70 ± 0.1 with the theoretical value of 1.67 for spencite and (Y, N)-apatite or yttrium silicon oxide nitride and with the value of 1.56 for yttrium oxide silicate, the measured value fits well with spencite and (Y, N)-apatite or yttrium silicon oxide nitride, although nitrogen could not be detected. The analysed calcium content of the secondary crystalline phase is lower than the calcium content of spencite. Thus the crystalline secondary phase in this Y_2O_3– Al_2O_3 (8–2 wt %)-doped hot-pressed silicon nitride with high calcium impurities can be identified as a spencite-(Y, N)-apatite solid solution.

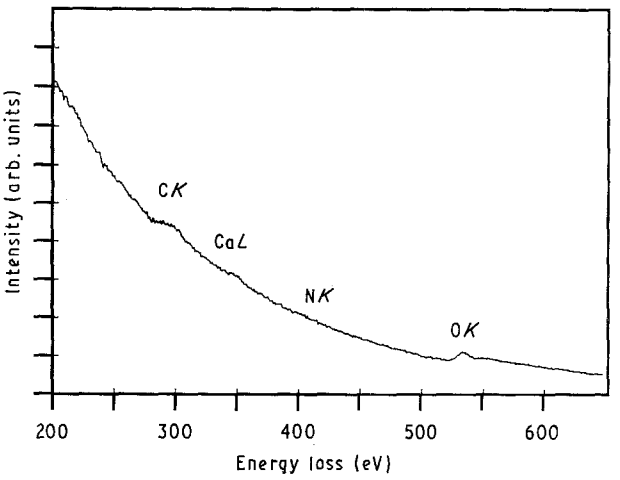

Figure 9 EELS spectrum of the crystalline secondary phase.

4. Conclusion

Microstructural and microanalytical investigations of an Y_2O_3–Al_2O_3-doped hot-pressed silicon nitride ceramic were performed to study the effects of post-sintering heat-treatments in an argon atmosphere.

The fracture surface investigations showed a change in the surface and internal morphology after the heat treatments. The amount of amorphous phase could be reduced, but a state of 100% crystallization could not be achieved. By analytical transmission electron microscopy the secondary phase was identified as a spencite-(Y-N)-apatite solid-solution, containing no aluminium, while aluminium was enriched in the residual glass. A SiAlON- mixed crystal formation could not be observed.

Acknowledgement

C.T.B. and K.K. thank the "Deutsche Forschungsgemeinschaft" for financial support under contract no. Kr 970/2.

References

1. C. C. AHN and G. THOMAS, *J. Amer. Ceram. Soc.* **66** (1983) 14.
2. O. L. KRIVANEK, T. M. SHAW and G. THOMAS, *ibid.* **62** (1979) 585.
3. L. K. V. LOU, T. E. MITCHELL and A. H. HEUER, *ibid.* **61** (1978) 392.
4. D. R. CLARKE, N. J. ZALUZEC and R. W. CARPENTER, *ibid.* **64** (1981) 601.
5. R. KOSSOWSKY, D. G. MILLER and E. S. DIAZ, *J. Mater. Sci.* **10** (1975) 983.
6. J. M. BIRCH and B. WILSHIRE, *ibid.* **13** (1978) 2627.
7. D. R. MOSHER, R. RAJ and R. KOSSOWSKY, *ibid.* **11** (1976) 49.
8. D. R. CLARKE, F. F. LANGE and G. D. SCHNITTGRUND, *J. Amer. Ceram. Soc.* **65** (1982) C-51.
9. L. K. L. FALK and G. L. DUNLOP, *J. Mater. Sci.* **22** (1987) 4369.
10. L. D. BENTSEN, D. P. H. HASSELMAN and T. Y. TIEN, *J. Amer. Ceram. Soc.* **67** (1984) C-85.
11. D. A. BONELL, T. Y. TIEN, M. RÜHLE, *ibid.* **70** (1987) 4460.
12. C. T. BODUR and K. KROMP, in "Brittle Matrix Composites 2", edited by A. M. Brandt and I. H. Marshall (Elsevier Applied Science, London, New York, 1988) p. 362.

13. H. SCHUMANN, in "Metallographie", 12th Edn (VEB Deutscher Verlag für Grundstoffindustrie, Leipzig, 1987) p. 57.
14. C. T. BODUR and K. KROMP, "Fortschrittsberichte der Deutschen Keramischen Gesellschaft" (Cfi: Ceramic Forum International), Vol. **3** (1988) p. 109.
15. R. R. WILLS, J. A. CUNNINGHAM, J. M. WIMMER and R. W. STEWART, *J. Amer. Ceram. Soc. Discuss. Notes* **59** (1976) 269.
16. W. E. LEE and G. E. HILMAS, *J. Amer. Ceram. Soc.* **72** (1989) 1931.
17. K. H. JACK, *J. Mater. Sci.* **11** (1976) 1135.
18. K. H. JACK, *Sci. Ceram.* **11** (1981) 125.

Received 30 September 1991
and accepted 11 August 1992